

Extended method for Statistical Signal Characterization using moments and cumulants: Application to recognition of pattern alterations in pulse-like waveforms employing Artificial Neural Networks

G. H. Bustos, H. H. Segnorile*

*Facultad de Matemática, Astronomía, Física y Computación (FAMAF), Universidad Nacional de Córdoba, M. Allende y H. de la Torre - Ciudad Universitaria, X5016LAE - Córdoba, Argentina.
Instituto de Física Enrique Gaviola - CONICET - Córdoba, Argentina.*

Abstract

We propose a statistical procedure to characterize and extract features from a waveform that can be applied as a pre-processing signal stage in a pattern recognition task using Artificial Neural Networks. Such a procedure is based on measuring a 30-parameters set of moments and cumulants from the waveform, its derivative, and its integral. The technique is presented as an extension of the Statistical Signal Characterization method existing in the literature.

As a testing methodology, we used the procedure to distinguish a pulse-like signal from different versions of itself with frequency spectrum alterations or deformations. The recognition task was performed by single feed-forward back-propagation networks trained for the case Sinc-, Gaussian-, and Chirp-pulse waveform. Because of the success obtained in these examples, we can conclude that the proposed extended statistical signal characterization method is an effective tool for pattern-recognition applications. In particular, we can use it as a fast pre-processing stage in embedded systems with limited memory or computational capability.

Keywords: statistical characterization, artificial neural networks, signal processing, real-time systems

1. Introduction

The first step in a signal-processing or pattern-recognition task is feature extraction. Diverse techniques are commonly used in such a process; fast Fourier transform (FFT) and convolution are traditional tools to detect a particular signal profile and extract information about its properties [1, 2, 3, 4]. Other methodologies are based on extracting statistical parameters, like measuring moments or cumulants [5, 6, 7, 8, 9, 10, 11, 12,

*Corresponding author

Email address: segnorile@famaf.unc.edu.ar (H. H. Segnorile)

Preprint submitted to Elsevier

January 2, 2023

13, 14, 15, 16], or the statistical signal characterization (SSC) procedure developed by H.L. Hirsch [5, 6]. These techniques are usually implemented as a pre-processing stage in Artificial Neural Networks (ANN).

FFT brings a complete representation of the signal, and convolution permits matching signals that are shifted or scaled in amplitude, but the operational cost is of the order of $N_s \log_2(N_s)$ [17], where N_s is the number of signal samples. On the other hand, the cost of extracting a statistical parameter is proportional to N_s ; however, there isn't a direct method to determine the type and amount of different parameters needed for suitably characterizing a signal. In general, such parameters are established empirically; and they depend on the signal complexity and the type of recognition task. In particular, the SSC technique is based on the extremum values of a function [5], and it has a poor performance when there is a lower amount of such extrema; besides, the few numbers of extracted parameters (4 for SSC) could be insufficient to perform the pattern recognition task in several signal cases. However, the simplicity and lower operational cost make statistical algorithms attractive to be used in embedded systems or where there are limited resources.

In this work, we use statistical characterization by means of moments and cumulants to propose an extension of Hirsch's SSC method. We aim to develop a systematic and fast feature extraction method, useful to characterize pulse-form signals in a pattern-recognition task. Such signal forms are present in NMR (Nuclear Magnetic Resonance) [18, 19, 20, 21, 22, 23, 24, 25, 26, 27] or EPR (Electron Paramagnetic Resonance) [28] pulse techniques, MRI (Magnetic Resonance Imaging) [29, 30, 31] procedures, radar applications [32, 33, 34], communication techniques [35, 36, 37, 38, 39, 40, 41, 42, 43, 44, 45, 46, 47, 48, 49], etc., where shaped-pulses methods are used to perform different actions. Therefore, a measurement of the pulse quality will permit correcting some deviation and then achieving an efficient technique. Besides, the lower operational cost for statistical algorithms is an advantage in implementing this method on a demanded processing control or in a low-performance embedded system. Such statistical characterization can be used as an efficient pre-processing stage of a simple ANN to complete the recognition procedure.

The remainder of the paper is organized as follows: Section 2 presents a mathematical approach where we gather in the same context a characterization of functions using moments or cumulants and Hirsch's SSC method; accordingly, some auxiliary functions are obtained from the original ones and can be used in the parameter extraction process. We propose, in Section 3, a 30-parameters characterization method using SSC parameters and the cumulants of several auxiliary functions extracted from the signal and its derivative and integral. Such a method is suggested as an extension of Hirsch's SSC, and we call it Extended SSC (ESSC). We use, in Section 3.1, ESSC as a fast pre-processing stage of an artificial neural network (ANN) for a pattern-recognition task. We use that recognition algorithm to discriminate between different versions of a pulse-like signal, where these versions are the original signal itself and several copies of it, which are affected by some deformation. We define, in Section 3.2, three of those recognition problems, where they present a Sinc, Gaussian, and Chirp function as the original signal. Then, in Section 3.3, we show the results and performance measurements of the ESSC method applied to these problems using confusion matrices, defining a sensitivity measurement, and applying the ReliefF algorithm. Finally, in Section 4, we present the discussions and

conclusions of this work.

2. Mathematical approach

The statistical characterization procedure used in this work relies on the following premise, *the extraction of a few representative parameters of a signal by applying statistical calculations over the signal itself or an unambiguous auxiliary one*. In this section, we develop such a premise to put in the same context the characterization of functions using moments or cumulants and the Hirsch's SSC method.

We define an auxiliary signal as a function extracted from the original one by using some mathematical method, as can be seen from Fig. 1. In that figure is shown different auxiliary functions g obtained from the signal $f(t_n)$, where the independent discrete real variable t_n is normalized to range between 0 and 1. Hereafter, we use independent discrete variables, but the concepts can also apply to continuous ones. For instance, in Fig. 1

- is shown $g(t_n) = f(t_n) / \sum_n |f(t_n)|$ which is equal that the original function but multiplied by a constant (the inverse of the sum of absolute values), and it can be interpreted as a weight function of the variable t_n ;
- we have $g(t_n) = |f(t_n)| / \sum_n |f(t_n)|$ that is equivalent to a probability density function (PDF) of t_n ;
- the function $g(f)$ is a histogram of the amplitude values of f (within range of t_n) normalized as a PDF, where each histogram interval has a width of around 1% of the whole amplitude range $[-0.22, 1]$;
- is represented a series of segments bounded by the extrema of the signal where the set of amplitude and time intervals $g[m] = (A_m, T_m)$ characterize the function $f(t_n)$, this procedure is part of the Hirsch's SSC method [5, 6].

The auxiliary functions adequately represent the original signal in a pattern recognition or discrimination problem if they can be unambiguously assigned from the set of signals that we want to discriminate.

To characterize $f(t_n)$ we could extract several parameters from its auxiliary function g . Accordingly, we may apply the discrete-time Fourier transform expression [50] to the functions in Fig. 1 (a) and (b), this is

$$\hat{g}(\omega) \equiv \sum_n g(t_n) e^{-i\omega t_n} = \sum_{q=0}^{\infty} \frac{(-i\omega)^q}{q!} \langle t^q \rangle, \quad (1)$$

where $t_n \equiv n \Delta t$ is the independent discrete variable, with $n \in \mathbb{N}_0$ and Δt is the sampling step time of the function g . In Eq. (1), we defined the q -th order moments

$$\langle t^q \rangle \equiv \sum_n g(t_n) t_n^q = \lim_{\omega \rightarrow 0} i^q \frac{d^q \hat{g}(\omega)}{d\omega^q}, \quad (2)$$

with $d^0 \hat{g}(\omega) / d\omega^0 \equiv \langle t^0 \rangle = \sum_n g(t_n) = \hat{g}(0)$. Then, to obtain $g(t_n)$ from (1) we can use the inverse transform

$$g(t_n) = \frac{\Delta t}{2\pi} \int_{-\pi/\Delta t}^{\pi/\Delta t} d\omega \hat{g}(\omega) e^{i\omega t_n}. \quad (3)$$

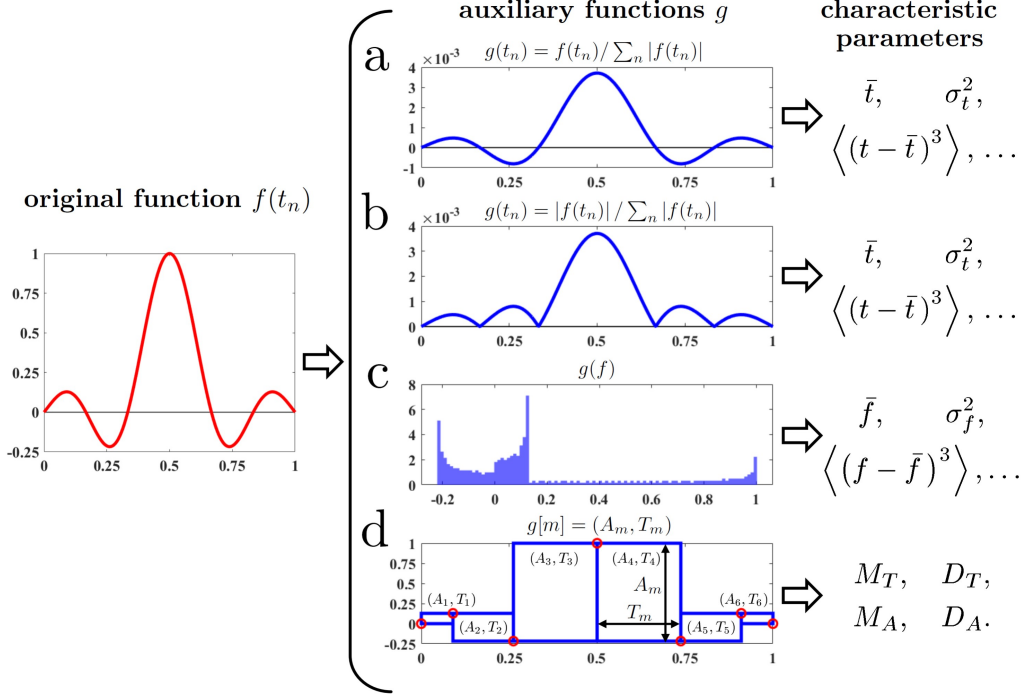


Figure 1: Examples of different mathematical methods to obtain auxiliary functions g and characteristic parameters from an original function or signal $f(t_n)$ (the time t is normalized to range between 0 and 1). a: weight function $g(t_n) = f(t_n) / \sum_n |f(t_n)|$; b: probability density function $g(t_n) = |f(t_n)| / \sum_n |f(t_n)|$; c: amplitude histogram $g(f)$ (with an interval width of around 1% of the whole amplitude range $[-0.22, 1]$); d: $g[m] = (A_m, T_m)$ is the set of amplitude and time segments bounded by the extrema of the signal (SSC method developed by Hirsch).

On the other hand, Eq. (1) can be written as the following expansion [51]

$$\hat{g}(\omega) = \exp \left[\sum_{q=1}^{\infty} \frac{(-i\omega)^q}{q!} c_q \right] + \langle t^0 \rangle - 1, \quad (4)$$

where c_q are the cumulants whose first values are defined as follows

$$\begin{aligned} c_1 &\equiv \langle t \rangle \equiv \bar{t}, & c_2 &\equiv \langle t^2 \rangle - \langle t \rangle^2 = \langle (t - \bar{t})^2 \rangle \equiv \sigma_t^2, \\ c_3 &\equiv \langle t^3 \rangle - 3 \langle t \rangle \langle t^2 \rangle + 2 \langle t \rangle^3 = \langle (t - \bar{t})^3 \rangle, \\ c_4 &\equiv \langle t^4 \rangle - 4 \langle t \rangle \langle t^3 \rangle - 3 \langle t^2 \rangle^2 + 12 \langle t \rangle^2 \langle t^2 \rangle - 6 \langle t \rangle^4 = \langle (t - \bar{t})^4 \rangle - 3 \langle (t - \bar{t})^2 \rangle^2, \end{aligned} \quad (5)$$

with \bar{t} and σ_t as the mean value and the standard deviation of the variable t_n under the weight function $g(t_n)$. In Eq. (5), we wrote the cumulants as functions of the moments

(2) or the q -th order central moments

$$\langle (t - \bar{t})^q \rangle \equiv \sum_n g(t_n) (t_n - \bar{t})^q. \quad (6)$$

Therefore, we can use the cumulants (5), or the central moments (6), or the moments (2) to define a set of characteristic parameters representing the original function, as usually found in the bibliography. This representation of the signal is important because such parameters are associated with the general properties of the functions. For instance, as it is known, the first moment or mean \bar{t} quantifies the average time where the amplitudes are equally distributed around it; the second central moment or variance σ_t^2 quantifies the spread out of the amplitudes from \bar{t} ; the third central moment or skewness $\langle (t - \bar{t})^3 \rangle$ quantifies the lopsidedness of the amplitude distribution values; the fourth central moment or kurtosis $\langle (t - \bar{t})^4 \rangle$ quantifies the heaviness of the tail (values far from \bar{t}) of the amplitude distribution values, and so on. Moreover, we can approximate the auxiliary function keeping only the terms with lower-order moments or cumulants in (1) and (4) for small values of ω (or for values close to the multiples of $\pm 2\pi/\Delta t$). Hence, the lower frequency part of the spectrum of the auxiliary functions (and for frequencies $\omega \simeq \pm 2\pi m/\Delta t$, $m \in \mathbb{N}_0$) is characterized by the lower-order parameters of Eq. (5) and we could use them as a tool to identify or discriminate different signals. For example, in the particular case of a gaussian signal the only non-null cumulants are $c_1 \equiv \bar{t}$ and $c_2 \equiv \sigma_t^2$ (with $\langle t^0 \rangle = 1$), and we can completely characterize this function with these two parameters.

In the following, we describe other parameters that could be used to characterize the function $f(t_n)$. In such a way, we may define the q -th order amplitude central moments

$$\langle (f - \bar{f})^q \rangle = \frac{1}{N} \sum_n (f(t_n) - \bar{f})^q, \quad (7)$$

with the mean value $\bar{f} \equiv \frac{1}{N} \sum_n f(t_n)$ and N is the number of time samples t_n . Besides, we have the variance $\sigma_f^2 \equiv \langle (f - \bar{f})^2 \rangle$. If the amplitude range of $f(t_n)$ is divided into segments of dimension Δf and we define $\alpha(f)$ as the number of samples that have values between f and $f + \Delta f$, we could approximate

$$\langle (f - \bar{f})^q \rangle \simeq \frac{1}{N} \sum_f \alpha(f) (f - \bar{f})^q = \Delta f \sum_f g(f) (f - \bar{f})^q, \quad (8)$$

where the sum is performed over the amplitude initial values of the segments. In (8), we defined $g(f) \equiv \alpha(f)/(N \Delta f)$ as representing a probability density function (PDF) of the amplitude of $f(t_n)$. We can note that, the smaller the value of Δf , the better the approximation (8) will be.

The expression (8) permits the link between the amplitude central moments (7) and $g(f)$, similarly that in Eq. (4). Thus, the Fourier transform of $g(f)$ can be developed in such amplitude moments. Then, $g(f)$ could represent an auxiliary function of $f(t_n)$, where the moments (7) and the mean value \bar{f} characterize $f(t_n)$, as is shown in Fig. 1 (c).

As a final analysis of signal characterization procedures, we present the SSC method developed by Hirsch [5, 6]. In this method, we obtain a series of segments bounded by the extrema of a signal as shown in Fig. 1 (d) (in the figure, the extrema are represented by circles). Then, we extract the amplitudes A_m and the time intervals T_m of the m -th segment and calculate the following set of mean values or SSC parameters

$$\begin{aligned} M_A &= \sum_{m=1}^{N_M} A_m / N_M, & M_T &= \sum_{m=1}^{N_M} T_m / N_M, \\ D_A &= \sum_{m=1}^{N_M} |A_m - M_A| / N_M, & D_T &= \sum_{m=1}^{N_M} |T_m - M_T| / N_M, \end{aligned} \quad (9)$$

where N_M is the total number of segments of the function.

We can analyze this method similar that the rest of the characterization procedures presented in Fig. 1. Accordingly, we could consider the set of segments $g[m] = (A_m, T_m)$ as an auxiliary function; where the parameters (9) are related with the first and central second moment of the amplitude and time segments. On the other hand, we could try to rebuild the original signal by the interpolation of the extrema using, for example, linear, polynomial, or sinusoidal functions. Thus, such a set of extrema contains relevant information about $f(t_n)$. Moreover, the variation of the amplitude and time segments is associated with the amplitude and frequency modulation of a signal, respectively; then, we can see that the SSC parameters characterize such modulation behaviors.

Finally, we conclude that a signal can be characterized by the statistical moments (2), (6) or (7), the cumulants (5), or the SSC parameters (9). The precision of such signal characterization depends on the number and relevance of these parameters (for instance, the influence of a particular moment in (1) or (4)). We can note that the calculation of these statistical parameters involves a sum or operation over the N_s -sampled values of $f(t_n)$ (to the computation of the SSC parameters is necessary to explore all the samples to detect the extrema of the function). That means their computational strength is $\propto N_s$, which is very light compared with other techniques, like convolution, Discrete Fourier Transform (DFT), or Fast Fourier Transform, whose take a strength $\propto N_s^2$ or $\propto N_s \log_2(N_s)$ [5]. Therefore, these statistical methods are adequate to be applied in embedded systems with limited computational capability or in real-time systems when a very-fast procedure is required to characterize different signals.

In the next section, we apply the statistical characterization method to a pattern recognition problem, using such a method as a pre-processing stage in Artificial Neural Networks (ANN).

3. Application to pattern recognition using neural networks

In this section, we apply the statistical characterization methods discussed in Section 2 as a fast pre-processing stage of an ANN used in a pattern recognition task. In particular, we want to characterize and discriminate different pulse-like signals, which

are waveforms of a bounded time duration used in various electronics areas like radar applications, NMR techniques, MRI, pulse shaping in telecommunications, etc. Moreover, we want to distinguish between a pulse signal and different versions of it with frequency spectrum alterations or deformations. These pulse deformations simulate non-idealities in the amplifiers or communication channel (then we could modify the original signal to compensate for such alterations).

Exhaustive training of an ANN is relevant to have success in applying it to solve a task. Thus, a fast and properly pre-processing strategy is necessary, particularly in real-time processing and when the network is used in embedded systems with memory restrictions or limitations. Therefore, we use the method of Section 2 for the auxiliary functions in Fig. 1 (a) and (c), but keeping only the three first cumulants (5), i.e. we characterize a pulse waveform with its mean value, variance and skewness of the time and amplitude distribution of $f(t_n)$. Besides, we also incorporate the SSC parameters of Fig. 1 (d) to characterize the amplitude and frequency modulation of the waveform. Accordingly, using similar nomenclature that in Eq. (9), we define the set of ten statistical parameters

$$\begin{aligned} \mathcal{P}(f) = & \left\{ M_T, D_T, M_A, D_A, \right. \\ & M_f^1 \equiv \bar{f}, D_f^2 \equiv \sigma_f^2, D_f^3 \equiv \langle (f - \bar{f})^3 \rangle, \\ & \left. M_t^1 \equiv \bar{t}, D_t^2 \equiv \sigma_t^2, D_t^3 \equiv \langle (t - \bar{t})^3 \rangle \right\}. \end{aligned} \quad (10)$$

We could also extract the high- and low-frequency behaviour of $f(t_n)$ by means of its derivative or integral, respectively. These operation are simply defined as the difference and the accumulation

$$\begin{aligned} f_D(t_n) & \equiv f(t_{n+1}) - f(t_n), \text{ with } f_D(t_{N+1}) = 0, \\ f_I(t_n) & \equiv f_I(t_{n-1}) + f(t_n), \text{ with } f_I(t_0) = 0, \end{aligned} \quad (11)$$

for discrete variables ($n \in [1, N]$). Then, the strength to compute the derivative f_D and the integral f_I is $\propto N$; thus, we could incorporate them as auxiliary functions to extract parameters and characterize f without an excessive computational effort.

In this way, we propose to use the set of parameters (10) calculated from the functions f , f_D , and f_I as an statistical characterization of $f(t_n)$. Therefore, that 30-parameters set can be consider as a “fingerprint” of the signal or original function, and we are naming this method as Extended Statistical Signal Characterization (ESSC), where it is proposed as an extension of the Hirsch’s SSC one. Such a pre-processing stage of the ANN, using the ESSC method for our pattern recognition problem, is shown in Fig. 2 and is explained in Section 3.1.

In the following sections, we apply the ESSC parameters to train an ANN for discriminating between an original pulse and other ones with frequency spectrum alterations.

3.1. ANN training by means of ESSC parameters

The process detailed in Fig. 2 shows the signal- or pattern-recognition method used to train an ANN with the ESSC parameters.

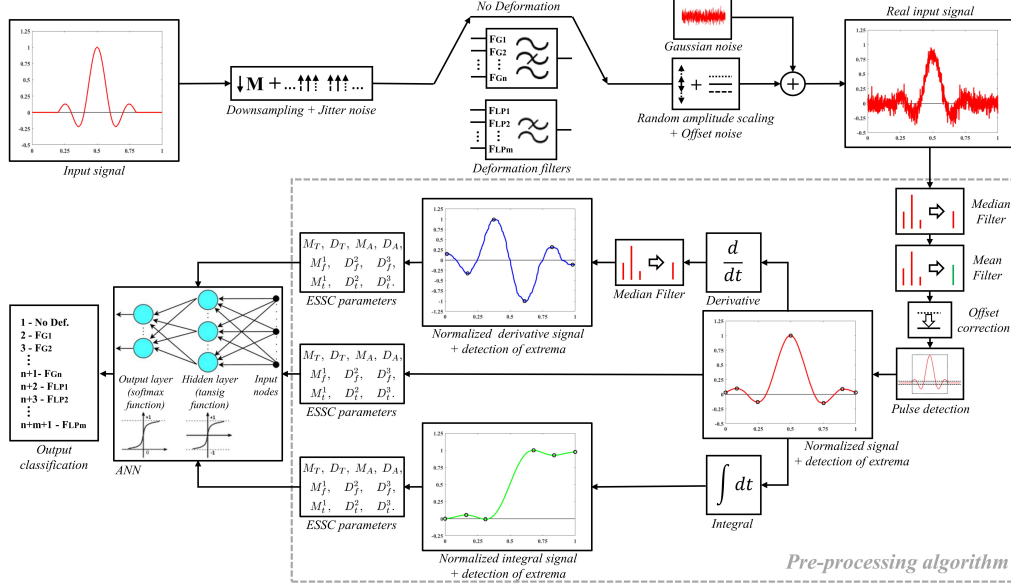


Figure 2: Schematic of the pre-processing algorithm of the artificial neural network for the pattern-recognition method.

First, we generate an ideal pulse *input signal* with a time resolution of 10000 points. Such an ideal signal passes through a *downsampling* stage where the samples are reduced by a factor of $M = 10$ (decimation) and is applied a uniform-random time *jitter noise* (between 0 and 9 samples) aimed at emulating the effects of an acquisition process. After that, we apply a *deformation filter* F_X (with X representing low-pass, band-pass, etc.) on the signal, simulating a spectral alteration due to non-idealities in the transmission channel, or the signal passes with *no deformation*. This filter stage aims to train the ANN with a set of knowing deformations (or no deformation) of the signal and then to recognize them. Following the filter stage, we perform a uniform-random *amplitude scaling* (up to 75% of the maximum value), and an *offset noise* introduces a uniform-random continuous level (up to 5% of the maximum amplitude value). Then, the *real input signal* is finally obtained by adding a *Gaussian white noise* (between 10 dB and 25 dB), and we have a simulation of a real acquired signal with deformation (or not) to feed the pre-processing algorithm of the ANN.

As was commented in Section 3, we aim to build a pre-processing algorithm where the computational strength is $\propto N$. Such an algorithm is detailed in Fig. 2 by the sequence of stages applied to the real input signal, which are inside the dashed rectangle. In an initial step, a noise cleaning of the signal is performed by two fast-filter stages; first, a *median filter* is especially used to clean spike noise; then, a *mean filter* (or moving average filter) completes the smoothing of the function form. These moving filters are applied using windows or arrays with few elements (around 40 for the median and 100 for the mean); where such windows are moved through all the samples of the function.

Following, an *offset correction* is applied to fix the continuous level of the signal; this is performed by extracting the average value at each end of the signal (in a window of 100 elements). After these noise cleaning procedures, we perform a *pulse detection* routine to extract a time and amplitude normalized form of the signal; in which the starting and ending time of the function is obtained by detecting where the absolute value of the amplitude exceeds a threshold around the 0-line (we used a 3% of the maximum absolute value as threshold); then, these extreme values of time are reassigned as 0 and 1.

The output of the pulse detection stage is the *normalized signal* used to characterize the waveform, and a routine of *detection of extrema* is applied to this signal. The obtained extrema (circles in the normalized signal waveform of Fig. 2) are used to calculate the SSC parameters of Eq. (9); then, we obtain ten *ESSC parameters* of the signal calculating the first order cumulants (see Eq. (10)). The statistical characterization of the waveform is completed by calculating the *derivative* and *integral* from the normalized signal, and after that by obtaining from each result the *ESSC parameters*. Such proceedings are detailed in the branches showing the *normalized derivative signal* and the *normalized integral signal* waveforms; where we applied the same routine for extracting the statistical parameters than in the normalized signal (with the extrema values shown as circles in the waveforms). We note that is applied another *median filter* after the derivative routine (this filter has a window of around 20 elements); it aims to clean some spike in the ends of the derivative function produced by the pulse detection stage, where the signal may present a step-function form due to the normalization in time.

The 30-parameters set characterizes the signal waveform; it is the input to the ANN. An integer number is the *output classification* of the neural network; this number identifies the different deformations of the signal (i.e., the type of used filter) or if the input is a waveform with no deformation.

An equal input signal, with the same choice of deformation filter (or with no deformation), produces different real input signals in the pre-processing algorithm due to the randomness included by different noise sources. Therefore, the training of the ANN is performed by exhaustively running this algorithm.

In the next section, we propose several simple examples of recognition of pulses and deformations to analyze the performance of a feed-forward ANN using the proposed pre-processing algorithm.

3.2. Application examples of pattern recognition

We are concerned with testing the feasibility of our pre-processing method of Fig. 2, using ESSC parameters as inputs in a single feed-forward ANN to characterize pulse waveforms. In order of that, we propose three recognition problems with the pulse form of a Sinc, a Gaussian, and a Chirp function, which are shown in (a.1) of Figs. 3, 4, and 5, respectively. Thus, we study an example where the waveform has amplitude modulation with oscillation (Sinc), without oscillation (Gaussian), and with frequency modulation (Chirp). The waveforms in (a.1) have their normalized amplitude spectra shown in (a.2), where the time (t) and frequency (ν) scales are reciprocal and arbitrary (e.g., if we have ms in t , then we obtain kHz in ν , and so on).

We chose two types of filters to apply deformations on the original pulses; one with a low-pass response and another with a sort of stop-band response that we called ‘Gaussian’. We name a filter with low-pass behavior as F_{LP} and a Gaussian one as F_G for the

sake of brevity. The frequency response of an F_{LP} is configured by the following function

$$G_{F_{LP}}(\nu) \equiv \frac{1}{2} [\tanh(SR_\nu(\nu + \nu_c)) - \tanh(SR_\nu(\nu - \nu_c))], \quad (12)$$

where ν_c is the characteristic frequency, and SR_ν is the ‘slew rate’ of the tanh profile. We want to emulate with an F_{LP} the high-frequency amplitude attenuation of an amplifier or transmission channel.

On the other hand, the frequency response of F_G is configured by

$$G_{F_G}(\nu) \equiv 1 - \frac{\Delta_a}{\max|G_g(\nu)|} G_g(\nu), \quad (13)$$

where

$$G_g(\nu) \equiv e^{-(\nu+\nu_c)^2/(2\sigma_\nu^2)} + e^{-(\nu-\nu_c)^2/(2\sigma_\nu^2)},$$

ν_c and σ_ν are the characteristic frequency and the standard deviation of the Gaussian profile, respectively. In Eq. (13), $\max|G_g(\nu)|$ is the maximum absolute value of the function $G_g(\nu)$, and Δ_a is the factor of maximum attenuation (ranged between 0 and 1). The F_G profile emulates an irregular or no-flat amplitude response of an amplifier or transmission channel.

To test the feasibility of our pre-processing algorithm, we use two sets of low-pass and Gaussian filters for each recognition problem (with Sinc, Gaussian, and Chirp waveform). In Figs. 3, 4, and 5, we show the filter responses in a dotted (green) line in (b.2, c.2, d.2, and e.2), where we indicate the parameters of the function (12) and (13). The deformed signal is obtained by multiplying the original amplitude spectrum (a.2) times the filter response and applying the inverse Fourier transform on the product. Therefore, in our recognition problems, we have the no-deformed signal (a.1 - ND) with its amplitude spectrum (a.2) and the deformed-by-filter signals (b.1 - F_{G1} , c.1 - F_{G2} , d.1 - F_{LP1} , and e.1 - F_{LP2}) with their spectra shown in solid (blue) line in (b.2, c.2, d.2, and e.2). In this way, we propose these basic recognition pattern examples to test the performance of our algorithm in a first instance, where there are lightly and heavily deformed signals.

In the next section, we analyze the behavior of a feed-forward back-propagation ANN aimed to solve the proposed pattern-recognition problems and the performance of the ESSC method, showing the obtained results.

3.3. Results for the examples of pattern recognition

In this section, we apply the algorithm of Fig. 2 to recognize several pulse waveforms affected by different spectral deformations. In this way, we implement a feed-forward back-propagation ANN to solve the pattern-recognition examples proposed in Section 3.2. The ESSC method proposed in Section 3, as an extension of the SSC technique, has a very-fast execution algorithm (similar to SSC). However, the included ‘extra’ parameters of the former method permit successfully characterize signals in which the last fails. To compare the performance of both methods, justifying the use of more parameters, we try to solve the problems of Section 3.2 using the 30- and 4-parameters (ESSC and SSC) techniques. We note that in the SSC method is common to use acceptance windows with statistical parameters to discriminate between different input signals [5, 9]; however, in the proposed examples, we observe there is a superposition between the ranges

of variation of such 4-parameters for the inputs affected by noise; thus, it is not possible to distinguish between signals using these windows. On the other side, in the ESSC method with 30 parameters is extremely difficult to configure a set of acceptance windows. Therefore, we choose to use an ANN in both methods as the strategy to solve our pattern recognition problems.

The ANN structure (see the ANN block in Fig. 2) is formed by an input layer with 30 or 4 nodes; this amount corresponds to the ESSC or SSC parameters entries. Then, a hidden layer has between 5 and 40 neurons with a *tansig* activation function. Finally, an output layer includes neurons and output terminals as the number of classes to be predicted; in our case, it is 5 (ND, FG1, FG2, FLP1, and FLP2). Such output neurons use the *softmax* activation function and implement the *one-hot encoding method*. The softmax's output is a 5-elements array with the prediction level for each class; this is a range of values between 0 and 1. Such a level is the probability of association of the input parameters with such a class; thus, we use a random selection weighted by these probabilities to choose the output class for that input (i.e., the output result of the ANN). We executed for each output class the algorithm of Fig. 2 and generated a set of 1000 elements or arrays of 30- or 4-parameters (5000 elements in total) for the training process. Besides, we use a Gaussian White Noise (GWN) source with zero mean and the standard deviation σ_N set as 5% of the maximum signal amplitude ($|f|_{max}$). Then, we obtain an ANN for each recognition problem (Sinc, Gaussian, and Chirp).

To select the number of neurons in the hidden layer (N_{hl}), we trained the network with a different quantity of hidden neurons ranging between 5 and 40 and with steps of 5. The criterion used to select such a range is to have a minimum and increment equal to the number of output neurons and a maximum with an order of magnitude higher than the minimum (we choose this maximum as a limit to the computational strength). Then, we evaluate the average *cross-entropy*, defined as

$$\overline{CE} \equiv -\frac{1}{M_t} \sum_{j=1}^{M_t} \sum_{i=1}^{M_c} [d_{ij} \ln(y_{ij}) + (1 - d_{ij}) \ln(1 - y_{ij})],$$

where M_t is the number of training exercises (5000 in our case), M_c is the number of classes in the recognition problem (5 in our case), d_{ij} and y_{ij} are the target and predicted values for the i th class in the j th exercise, respectively. The values of d_{ij} can be 1 or 0 if the i th class is or is not the target class of the j th exercise, respectively. Such values are known for the input signals and provided to train the network. On the other hand, the values of y_{ij} range between 0 (slightly higher than 0) and 1. Besides, y_{ij} is the output of the ANN for the i th class in the j th exercise and is associated with the probability that the input signal belongs to class i . The entropy \overline{CE} is the mean value calculated from all the training exercises for each value of N_{hl} (this is for $M_t = 5000$ inputs parameters or signals). The internal configuration of an ANN, for a fixed amount of hidden neurons, changes in different training cycles due to its random initial configuration. Accordingly, we select the ANN configuration with minimum \overline{CE} (with the best performance) between 50 different training cycles for a fixed value N_{hl} (i.e., $\overline{CE}_{\{min\}}$). Such minimum value will be the cross-entropy assigned to a particular number of hidden neurons. Finally, to solve a recognition problem, we use the ANN configuration and the amount of N_{hl} hidden neurons with the lowest $\overline{CE}_{\{min\}}$ value between the tested range of N_{hl} . In Fig. 6,

we show the values of $\overline{\text{CE}}_{\{min\}}$ as a function of N_{hl} for the different pattern-recognition problems of Section 3.2 (Sinc, Gaussian, and Chirp), using the ESSC (30 parameters) and SCC (4 parameters) method. Therefore, from the results shown in Fig. 6, we will configure the following number N_{hl} of hidden neurons for each pattern: 30 (ESSC) and 10 (SCC) for the Sinc, 25 (ESSC) and 5 (SCC) for the Gaussian, and 35 (ESSC) and 30 (SCC) for the Chirp.

Following the ANN building, we use the network to analyze the performance of the pre-processing algorithm in our proposed examples. In our instances, the different *classes* (and their ID numbers) for the classification problems are ND (1), F_{G1} (2), F_{G2} (3), F_{LP1} (4), and F_{LP2} (5), for a no-deformed signal or the different deformed-by-filter ones, respectively. The outcome of the ANN is a number that identifies the input class type; that is, the result of a random selection weighted by the probability outputs of the softmax function, as was earlier commented. A successful class identification will occur if there is a matching between the output and input class. Therefore, we can test the ability of the network to recognize such a class by knowing the target class of the input and comparing it with the resulting output. Accordingly, the performance of a pattern-recognition exercise is reflected by using a *confusion matrix*, which indicates the number of times that an *output class* is obtained due to a fixed *target class*.

We perform the testing for the ESSC and SSC method under different GWN levels, for a Signal-to-Noise Ratio (SNR) ranging between 25 dB and 10 dB and with steps of 5 dB, where $\text{SNR} = 20 \log_{10} (|f|_{max} / \sigma_N)$ (approximately between a 5.6% and 31.6% ratio of $\sigma_N / |f|_{max}$). Accordingly, we used a dataset of 5000 elements or statistical parameters (1000 elements per class) for each pre-processing method and noise level (similar to the training dataset). The results are shown in Figs. 7, 8, and 9, respectively, for Sinc, Gaussian, and Chirp signals, and are analyzed in Section 4.

To conclude this section, we want to study how sensitive the ESSC method is to each parameter variation and how relevant the parameters are in the pattern recognition or classification process. Accordingly, we propose to measure the value of the output of the ANN when the studied parameter is altered, but the rest of the input parameters are set as the mean of their dataset values. Because the time and amplitude of the signal are normalized to 1, we can compare the outputs between different ESSC parameters if we divide the amplitude parameters by the following values: 2 for M_A and D_A (M_f^1 is not altered), 4 for D_f^2 , and 8 for D_f^3 (in general, we divide D_f^q by 2^q). Therefore, we use the trained network of the proposed recognition examples under a GWN with an SNR of 25 dB. Then, we take the dataset for a fixed input class and calculate the mean values of the input parameters. After that, we vary the chosen parameter from its mean value in steps of Δ_p and measure the ANN output value for the corresponding class. The parameter step is set with the exponential variation defined by $\Delta_p = \pm A e^{kn}$, with $n = \{1, 2, \dots, 30\}$, $k \equiv (\log(10) - \log(0.01))/29$, and $A \equiv 0.01 e^{-k}$, where we have $0.01 \leq |\Delta_p| \leq 10$. Finally, we take the value of $|\Delta_p|$ that the ANN output target class presents a value below 0.9 for the corresponding input class (the outcome will be close to 1 for a successful recognition task); we call such a value $|\Delta_p|_{90\%}$ and define the sensitivity as $s_p = 1/|\Delta_p|_{90\%}$ (thus, $0.1 \leq s_p \leq 100$).

The sensitivity results are shown in Figs. 10, 11, and 12, respectively, for Sinc, Gaussian, and Chirp-pulse. We perform a graph for each target class where we have a bar for the signal (middle red bar), derivative (left green bar), and integral (right blue bar).

Therefore, there are ten parameter names in the abscissa axis and three values per each one (the 30 ESSC parameters). We can observe from the results that the recognition or classification process is more sensitive to the ‘extended’ part of the ESSC parameters than the original 4-parameter SSC method. It is important to note that Fig. 11 shows saturation in the sensitivity for all the parameters in the cases with deformation filters F_{LP1} and F_{LP2} for the Gaussian example. This ‘pathology’ is coherent with the results from the CM of Fig. 8, which reflects the difficulty in distinguishing between those cases (see (d) and (e) from Fig. 4), and the algorithm is extreme-sensitive to fluctuations of all the input parameters. In such cases, the proposed 30-parameter methodology fails, and it would be necessary to include moments or cumulants of higher order.

On the other hand, we study the relevance of each parameter using the ReliefF algorithm [52, 53, 54, 55, 56, 57, 58]. We use the MATLAB® ReliefF function for classification, and the results for the recognition examples (with SNR of 25 dB) are shown in Fig. 13, where the parameter $K = 10$ for the nearest neighbors per class is set. The bar graphs are built the same way as in the sensitivity figures. A parameter is relevant if its value is greater than a threshold τ , which can be defined using Chebyshev’s inequality, as it is known. Then, for a given confidence level α , $\tau = 1/\sqrt{\alpha m}$ is good enough to make the probability of a Type I error less than α , where m is the number of random training instances used to define the ReliefF values. We use all the dataset values; thus, $m = 5000$. The higher values of ReliefF define the higher bound for τ (and the lower bound of α); then, it is approximately obtained $\tau = 0.41, 0.17$, and 0.46 (or $\alpha = 0.0012, 0.0069$, and 0.0009) for the Sinc, Gaussian, and Chirp examples, respectively. Thus, the best-obtained condition confines the error approximately below 0.1%. Besides, all the ReliefF values are positive. We can conclude that the 30 parameters are relevant in the proposed recognition or classification examples, with better or worse participation depending on the pattern to recognize or characterize. In particular, the lower values obtained for the Gaussian problem reflect the difficulty of this signal discrimination task (see Fig. 4).

4. Discussion and conclusion

In this work, we propose a 30-parameters pre-processing method to extract waveform features that can be applied in a pattern recognition task (Section 3). Such a method is based on the statistical characterization of the signal, using moments and cumulants of the waveform, its derivative, and its integral. The proposed technique is presented as an extension of the SSC method developed by H.L. Hirsch, so we call it ESSC. Because of the statistical calculation of the parameters, the ESSC technique is a very-fast procedure suitable for use in embedded systems with limited memory or computational power.

We can observe that a statistical parameter calculation consists of N_s sum operations where we can extract relevant features of a waveform (e.g. mean value, variance, skewness, kurtosis, etc.). On the other hand, in a complete spectrum calculation for DFT, there are N_s sum operations per each of the N_s coefficients or spectral components; this is an approximation of N_s^2 total operations (or $N_s \log_2(N_s)$ for the FFT algorithm). In general, we need the complete spectrum to extract some relevant waveform property; thus, this comparison of total operation between both methods evidences the advantage of the statistical characterization of the signal in pattern recognition problems.

From Figs. 7, 8, and 9, we conclude that the recognition performance decreases when the level of noise increases, as is expected; however, the 30-parameter ESSC method has a better performance than the 4-parameter SSC one in all the cases studied. In particular, the SSC technique has more difficulty recognizing the Gaussian-pulse waveform than the ESSC one at the high-SNR value of 25 dB. This SSC's poor performance is because there is a very low amount of extrema in the Gaussian form. Nevertheless, the Gaussian-pulse recognition problem presents similar waveforms between classes (see Fig. 4); thus, in this case, the discrimination process is a difficult task for both methods. On the other hand, in general, the ESSC methodology shows a very-good performance under an acceptable SNR of 25 dB. Besides, such good performance is present at SNR above 20 dB for the Sinc-pulse and above 15 dB for the Chirp-pulse recognition problem (where the waveform presents a frequency modulation).

The results of Figs. 10, 11, and 12 show that the class recognition or classification process is more sensitive to the 'extended' part of the ESSC parameters than the original 4-parameter SSC method. Besides, we can conclude from the ReliefF values of Fig. 13 that all 30 parameters are relevant in the discrimination signal process of the proposed examples. Nevertheless, the most relevant parameters differ from one waveform to other, and all the parameters contribute to a general waveform recognition procedure. On the other hand, if the recognition procedure of a waveform is not successful, we can extend even more the method and increase the number of ESSC parameters by adding higher order moments, cumulants, derivatives, or integrals, to improve the accuracy of such a procedure.

Finally, we found the proposed ESSC method (with 30 parameters or a more extended version) as an appropriate and very-fast tool for pre-processing and discriminating waveforms in pattern-recognition problems, particularly when the computational capabilities are limited.

5. Acknowledgement

This work was supported by CONICET and FONCYT (PICT 2013-2600), Agencia Nacional de Promoción de la Investigación, el Desarrollo Tecnológico y la Innovación (MINCYT). We thank Graciela Corral-Briones for helpful comments and discussions.

References

- [1] D. Nghia Do and S. Osowski. Shape recognition using FFT preprocessing and neural network. *COMPEL - The international journal for computation and mathematics in electrical and electronic engineering*, 17(5/6):658–666, 1998.
- [2] A. Hossen and U. Heute. A novel extension of the SB-FFT: Sub-segment inverse fast fourier transform (SS-IFFT) with different applications. *Journal of Computational Methods in Sciences and Engineering*, 13(3-4):361–375, 2013.
- [3] S. Hui and S.H. Żak. Discrete fourier transform based pattern classifiers. *Bulletin of the Polish Academy of Sciences: Technical Sciences*, 62(1):15–22, 2014.
- [4] S. Lin, N. Liu, M. Nazemi, H. Li, C. Ding, Y. Wang, and M. Pedram. FFT-based deep learning deployment in embedded systems. In *2018 Design, Automation & Test in Europe Conference & Exhibition (DATE)*, pages 1045–1050. IEEE, 2018.
- [5] H.L. Hirsch. *Statistical Signal Characterization*. Boston:Artech House, 1991.

- [6] H.L. Hirsch. Statistical signal characterization-new help for real-time processing. In *Proceedings of the IEEE 1992 National Aerospace and Electronics Conference@m_NAECON 1992*, volume 1, pages 121–127, 1992.
- [7] A. Pakhomov, A. Sicignano, M. Sandy, and E.T. Goldburt. Seismic footstep signal characterization. In E.M. Carapezza, editor, *Sensors, and Command, Control, Communications, and Intelligence (C3I) Technologies for Homeland Defense and Law Enforcement II*, volume 5071, pages 297–305. International Society for Optics and Photonics, SPIE, 2003.
- [8] A. Hossen, B. Al Ghunaimi, and M.O. Hassan. Statistical signal characterization of spectral analysis of heart rate variability for screening of patients with obstructive sleep apnea. *The Journal of Engineering Research [TJER]*, 3(1):1–9, 2006.
- [9] A. Hossen, F. Al-Wadahi, and J.A. Jervase. Classification of modulation signals using statistical signal characterization and artificial neural networks. *Engineering Applications of Artificial Intelligence*, 20(4):463–472, 2007.
- [10] K.C. Gryllias and I.A. Antoniadis. A support vector machine approach based on physical model training for rolling element bearing fault detection in industrial environments. *Engineering Applications of Artificial Intelligence*, 25(2):326–344, 2012. Special Section: Local Search Algorithms for Real-World Scheduling and Planning.
- [11] B. Esmael, A. Arnaout, R.K. Fruhwirth, and G. Thonhauser. A statistical feature-based approach for operations recognition in drilling time series. *International Journal of Computer Information Systems and Industrial Management Applications*, 4(6):100–108, 2012.
- [12] H.H. Segnorile, G.O. Forte, G.D. Farrher, and E. Anoardo. NMR-SSC magnetic field profiler applied to magnetic field shimming. *IEEE Latin America Transactions*, 11(1):257–262, 2013.
- [13] A. Hossen, Z. Al-Hakim, M. Muthuraman, J. Raethjen, G. Deuschl, and U. Heute. Discrimination of parkinsonian tremor from essential tremor by voting between different emg signal processing techniques. *Journal of Engineering Research*, 11(1):11–22, 2014.
- [14] C. Delpha, D. Diallo, H. Al Samrout, and N. Moubayed. Multiple incipient fault diagnosis in three-phase electrical systems using multivariate statistical signal processing. *Engineering Applications of Artificial Intelligence*, 73:68–79, 2018.
- [15] T.J. O’Shea, T. Roy, and T.C. Clancy. Over-the-air deep learning based radio signal classification. *IEEE Journal of Selected Topics in Signal Processing*, 12(1):168–179, 2018.
- [16] Xiaolin Zhang, Jianting Sun, and Xiaotong Zhang. Automatic modulation classification based on novel feature extraction algorithms. *IEEE Access*, 8:16362–16371, 2020.
- [17] W.H. Press, S.A. Teukolsky, W.T. Vetterling, and B.P. Flannery. *NUMERICAL RECIPES*, chapter 12,13. Cambridge University Press, third edition edition, 2007.
- [18] C. Bauer, R. Freeman, T. Frenkiel, J. Keeler, and A.J. Shaka. Gaussian pulses. *Journal of Magnetic Resonance (1969)*, 58(3):442–457, 1984.
- [19] W.S. Warren. Effects of arbitrary laser or NMR pulse shapes on population inversion and coherence. *The Journal of Chemical Physics*, 81(12):5437–5448, 1984.
- [20] J. Baum, R. Tycko, and A. Pines. Broadband and adiabatic inversion of a two-level system by phase-modulated pulses. *Phys. Rev. A*, 32:3435–3447, Dec 1985.
- [21] J. Friedrich, S. Davies, and R. Freeman. Shaped selective pulses for coherence-transfer experiments. *Journal of Magnetic Resonance (1969)*, 75(2):390–395, 1987.
- [22] H. Kessler, U. Anders, G. Gemmecker, and S. Steuernagel. Improvement of NMR experiments by employing semiselective half-Gaussian-shaped pulses. *Journal of Magnetic Resonance (1969)*, 85(1):1–14, 1989.
- [23] R. Freeman. Selective excitation in high-resolution NMR. *Chemical reviews*, 91(7):1397–1412, 1991.
- [24] H. Geen and R. Freeman. Band-selective radiofrequency pulses. *Journal of Magnetic Resonance (1969)*, 93(1):93–141, 1991.
- [25] S. Ding and C.A. McDowell. Multiple-quantum MAS NMR spectroscopy of spin-32 quadrupolar spin systems using shaped pulses. *Journal of Magnetic Resonance*, 135(1):61–69, 1998.
- [26] R. Freeman. Shaped radiofrequency pulses in high resolution NMR. *Progress in Nuclear Magnetic Resonance Spectroscopy*, 32(1):59–106, 1998.
- [27] R. Siegel, T.T. Nakashima, and R.E. Wasylshen. Signal enhancement of NMR spectra of half-integer quadrupolar nuclei in solids using hyperbolic secant pulses. *Chemical Physics Letters*, 388(4):441–445, 2004.
- [28] P.E. Spindler, P. Schöps, W. Kallies, S.J. Glaser, and T.F. Prisner. Perspectives of shaped pulses for EPR spectroscopy. *Journal of Magnetic Resonance*, 280:30–45, 2017.
- [29] R.J. Sutherland and J.M.S. Hutchison. Three-dimensional NMR imaging using selective excitation. *Journal of Physics E: Scientific Instruments*, 11(1):79–83, jan 1978.

- [30] J.M.S. Hutchinson, R.J. Sutherland, and J.R. Mallard. NMR imaging: image recovery under magnetic fields with large non-uniformities. *Journal of Physics E: Scientific Instruments*, 11(3):217–222, mar 1978.
- [31] P.A. Bottomley. Spatial localization in NMR spectroscopy in vivo. *Annals of the New York Academy of Sciences*, 508(1):333–348, 1987.
- [32] James D Taylor, editor. *Ultra-wideband radar technology*. CRC press, 2000.
- [33] L. Hanning. Pulse shaping of radar transmitters - Compensation of memory effects through digital pre-distortion. Master's thesis, Department of Electrical Engineering - CHALMERS UNIVERSITY OF TECHNOLOGY, SE-412 96 Gothenburg, Sweden, 2018.
- [34] H.-S. Cho and Y.-J. Park. Detection of heart rate through a wall using UWB impulse radar. *Journal of healthcare engineering*, 2018:4832605, 2018.
- [35] L.B. Michael, M. Ghavami, and R. Kohno. Multiple pulse generator for ultra-wideband communication using Hermite polynomial based orthogonal pulses. In *2002 IEEE Conference on Ultra Wideband Systems and Technologies (IEEE Cat. No. 02EX580)*, pages 47–51. IEEE, 2002.
- [36] I.S. Lin, J.D. McKinney, and A.M. Weiner. Photonic synthesis of broadband microwave arbitrary waveforms applicable to ultra-wideband communication. *IEEE Microwave and Wireless Components Letters*, 15(4):226–228, 2005.
- [37] M.-J. Hao and C.-H. Lai. Pulse shaping based PAPR reduction for OFDM signals with minimum error probability. In *2008 International Symposium on Intelligent Signal Processing and Communications Systems*, pages 1–4. IEEE, 2009.
- [38] S. Chattopadhyay and S.K. Sanyal. The effect of gaussian pulse-shaping filter roll-off factor on the performance of QPSK modulated system. In *2009 International Symposium on Signals, Circuits and Systems*, pages 1–4. IEEE, 2009.
- [39] S. Mohapatra. *A new approach for performance improvement of OFDM system using pulse shaping*. PhD thesis, Department of Electrical Engineering - National Institute of Technology Rourkela, Rourkela-769 008, Orissa, India, 2009.
- [40] R. Mehra and S. Devi. Area efficient & cost effective pulse shaping filter for software radios. *International Journal of Ad hoc, Sensor & Ubiquitous Computing (IJASUC) Vol.*, 1:85–91, 2010.
- [41] M. Pal. Algorithm for sharpening raised cosine pulse shaping digital filter and analysis of performance of QAM system when subjected to sharpened raised cosine filter. *International Journal of Scientific and Research Publications*, 2(1), 2012.
- [42] D.K. Sharma, A. Mishra, and R. Saxena. Effect of pulse shaping on ber performance of QAM modulated OFDM signal. *TECHNIA–International Journal of Computing Science and Communication Technologies*, 4(2):1–8, 2012.
- [43] J.M.G. Balsells, A. Jurado-Navas, M. Castillo-Vazquez, A.B. Moreno-Garrido, and A. Puerta-Notario. Advantages of solitonic shape pulses for full-optical wireless communication links. *Chin. Opt. Lett.*, 10(4):040101, Apr 2012.
- [44] D. Gandhi, S. Gupta, and U. Dalal. Implementation of pulse shaping techniques in OFDM system. *International Journal of Computer Applications*, 68(10):19–23, 2013.
- [45] M.A. Soto, M. Alem, M. Amin Shoaie, A. Vedadi, C.-S. Brès, L. Thévenaz T., and Schneider. Optical sinc-shaped Nyquist pulses of exceptional quality. *Nature communications*, 4(1):2898, 2013.
- [46] A.S. Karar, Y. Gao, J.C. Cartledge, S. Gazor, M. O'Sullivan, C. Laperle, A. Borowiec, and K. Roberts. Mitigating intra-channel nonlinearity in coherent optical communications using ISI-free polynomial pulses. In *OFC 2014*, pages 1–3. IEEE, 2014.
- [47] T.K. Roy, M.F. Pervej, and M. Morshed. Performance comparison of three optimized alternative pulse shaping filters with the raised cosine filter for wireless applications. In *2015 International Conference on Computer and Information Engineering (ICCIE)*, pages 9–12. IEEE, 2015.
- [48] D. Das. Peak to average power ratio reduction in OFDM using pulse shaping technique. *Computer Engineering and Applications Journal*, 5(2):57–64, 2016.
- [49] P.K. Yadav, V.K. Dwivedi, B.T. Maharaj, V. Karwal, and J.P. Gupta. Performance enhancement of 5G OFDM systems using modified raised cosine power pulse. *Wireless Personal Communications*, 106(4):2375–2386, 2019.
- [50] A.V. Oppenheim, A.S. Willsky, and S.H. Nawab. *Signals & systems*. Prentice-Hall International, Inc., 2nd edition, 1997.
- [51] L.E. Reichl. *A Modern Course in Statistical Physics*, chapter 4, pages 173–228. JOHN WILEY & SONG, INC., 2nd edition edition, 1998.
- [52] K. Kira and L.A. Rendell. The feature selection problem: Traditional methods and a new algorithm. In *AAAI-92 Proceedings*, volume 2, pages 129–134, 1992.
- [53] K. Kira and L.A. Rendell. A practical approach to feature selection. In D. Sleeman and P. Edwards,

- editors, *Machine Learning Proceedings 1992*, pages 249–256, San Francisco (CA), 1992. Morgan Kaufmann.
- [54] I. Kononenko. Estimating attributes: Analysis and extensions of relief. In F. Bergadano and L. De Raedt, editors, *Machine Learning: ECML-94*, pages 171–182, Berlin, Heidelberg, 1994. Springer Berlin Heidelberg.
 - [55] I. Kononenko, M. Robnik-Šikonja, and U. Pompe. Relieff for estimation and discretization of attributes in classification, regression, and ilp problems. *Artificial intelligence: methodology, systems, applications*, pages 31–40, 1996.
 - [56] I. Kononenko, E. Šimec, and M. Robnik-Šikonja. Overcoming the myopia of inductive learning algorithms with relieff. *Applied Intelligence*, 7:39–55, 1997.
 - [57] M. Robnik-Šikonja and I. Kononenko. Theoretical and empirical analysis of relieff and rrelieff. *Machine Learning*, 53:23–69, 2003.
 - [58] R.J. Urbanowicz, M. Meeker, W. La Cava, R.S. Olson, and J.H. Moore. Relief-based feature selection: Introduction and review. *Journal of Biomedical Informatics*, 85:189–203, 2018.

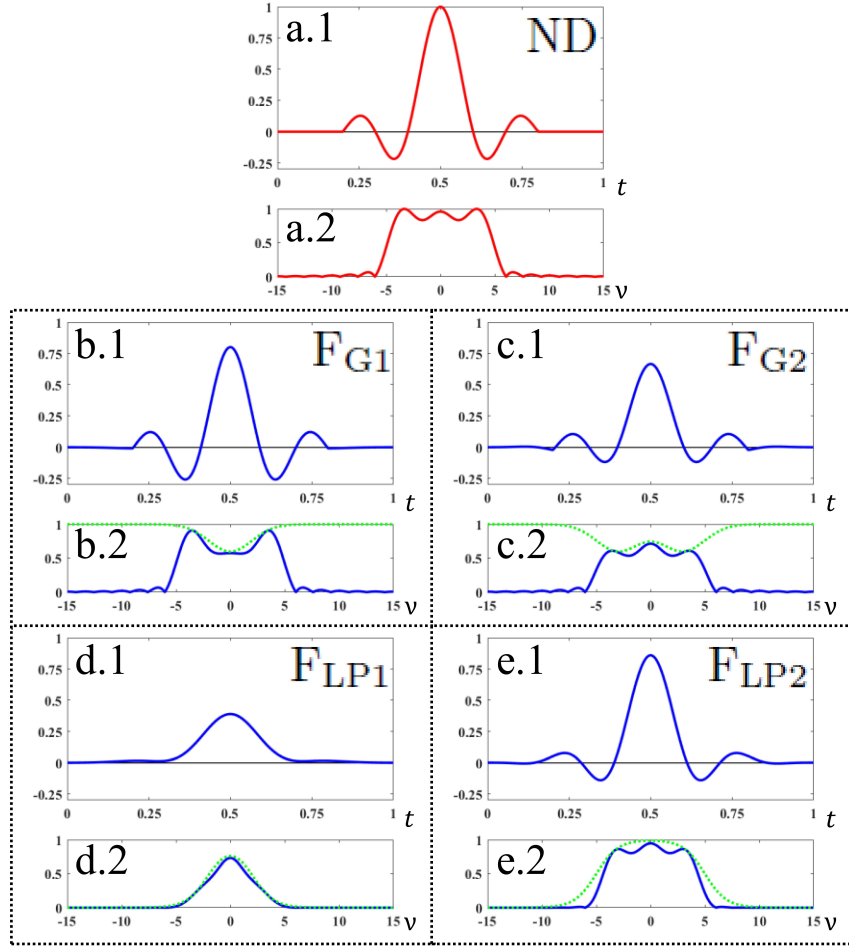


Figure 3: Deformation filters applied to a Sinc pulse. The original Sinc signal (a.1, no deformation) and its amplitude spectrum (a.2). It is shown the resulting signals (b.1, c.1, d.1, and e.1) and their corresponding amplitude spectra (solid blue line in b.2, c.2, d.2, and e.2) obtained by multiplying the original signal spectrum (a.2) times the deformation filter amplitude spectra (dotted green line in b.2, c.2, d.2, and e.2). The parameters for Gaussian and Low-Pass filters are the following, (b.2) F_{G1} : $\nu_c = 0$, $\sigma_\nu = 2$, $\Delta_a = 0.4$; (c.2) F_{G2} : $\nu_c = 3$, $\sigma_\nu = 2$, $\Delta_a = 0.4$; (d.2) F_{LP1} : $\nu_c = 2$, $SR_\nu = 0.5$; (e.2) F_{LP2} : $\nu_c = 5$, $SR_\nu = 0.5$.

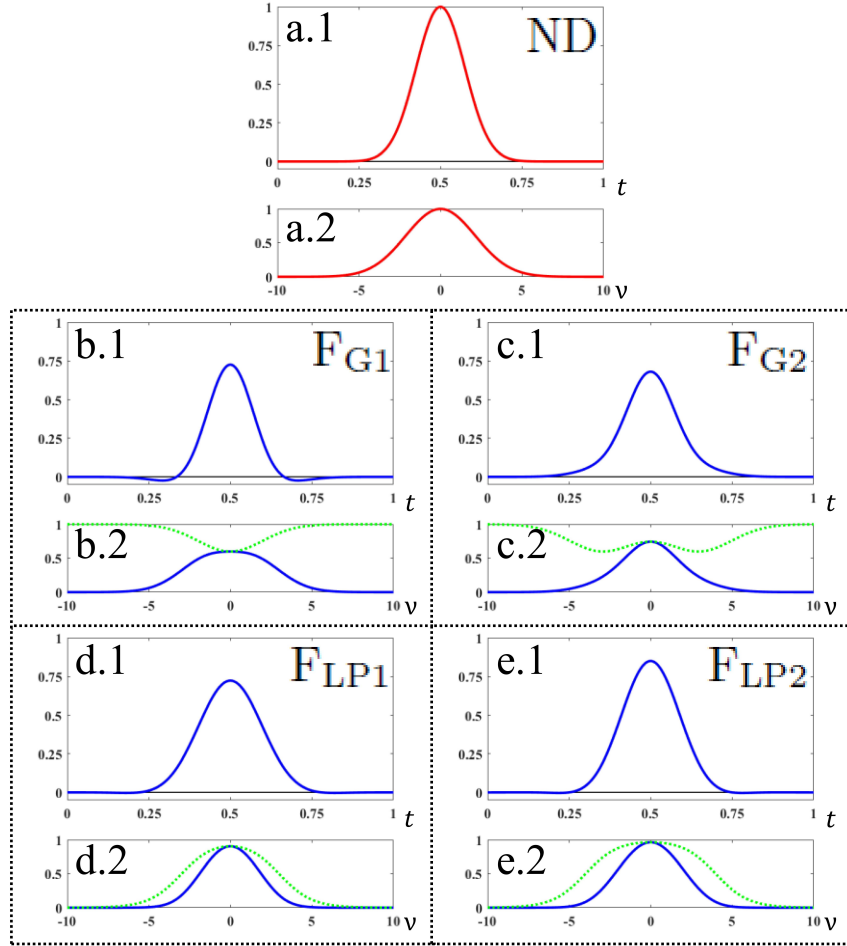


Figure 4: Deformation filters applied to a Gaussian pulse. The original Gaussian signal (a.1, no deformation) and its amplitude spectrum (a.2). It is shown the resulting signals (b.1, c.1, d.1, and e.1) and their corresponding amplitude spectra (solid blue line in b.2, c.2, d.2, and e.2) obtained by multiplying the original signal spectrum (a.2) times the deformation filter amplitude spectra (dotted green line in b.2, c.2, d.2, and e.2). The parameters for Gaussian and Low-Pass filters are the following, (b.2) F_{G1} : $\nu_c = 0$, $\sigma_\nu = 2$, $\Delta_a = 0.4$; (c.2) F_{G2} : $\nu_c = 3$, $\sigma_\nu = 2$, $\Delta_a = 0.4$; (d.2) F_{LP1} : $\nu_c = 3$, $SR_\nu = 0.5$; (e.2) F_{LP2} : $\nu_c = 4$, $SR_\nu = 0.5$.

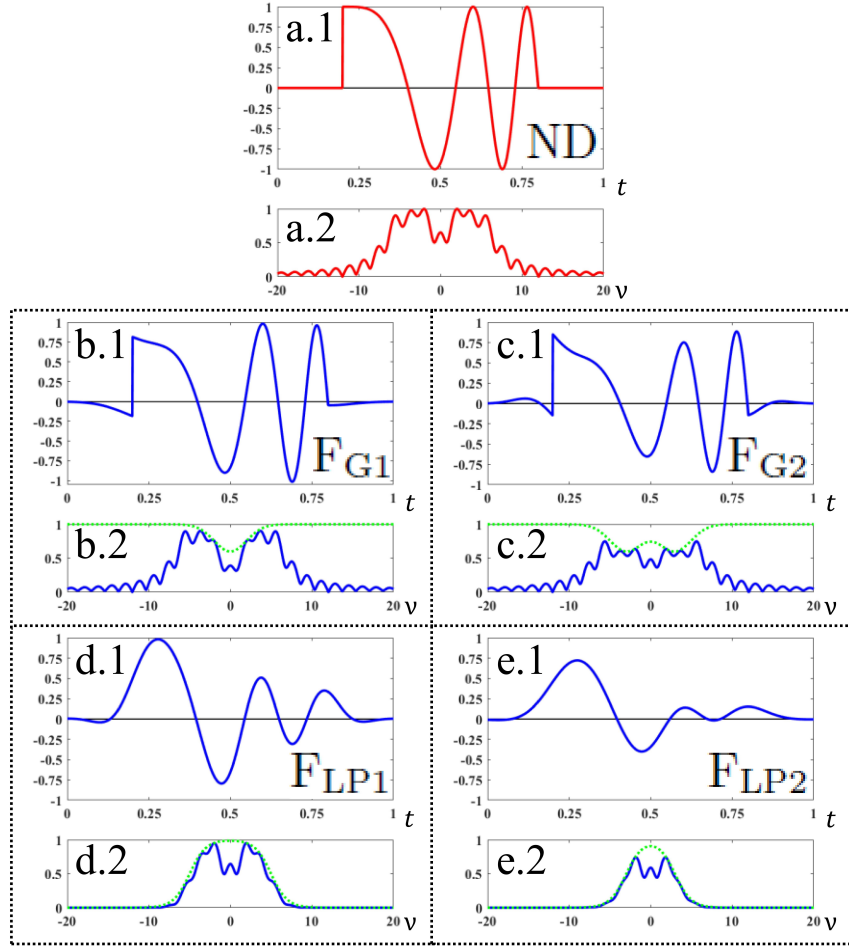


Figure 5: Deformation filters applied to a Chirp pulse. The original Chirp signal (a.1, no deformation) and its amplitude spectrum (a.2). It is shown the resulting signals (b.1, c.1, d.1, and e.1) and their corresponding amplitude spectra (solid blue line in b.2, c.2, d.2, and e.2) obtained by multiplying the original signal amplitude (a.2) times the deformation filter amplitude spectra (dotted green line in b.2, c.2, d.2, and e.2). The parameters for Gaussian and Low-Pass filters are the following, (b.2) F_{G1} : $\nu_c = 0$, $\sigma_\nu = 2$, $\Delta_a = 0.4$; (c.2) F_{G2} : $\nu_c = 3$, $\sigma_\nu = 2$, $\Delta_a = 0.4$; (d.2) F_{LP1} : $\nu_c = 5$, $SR_\nu = 0.5$; (e.2) F_{LP2} : $\nu_c = 3$, $SR_\nu = 0.5$.

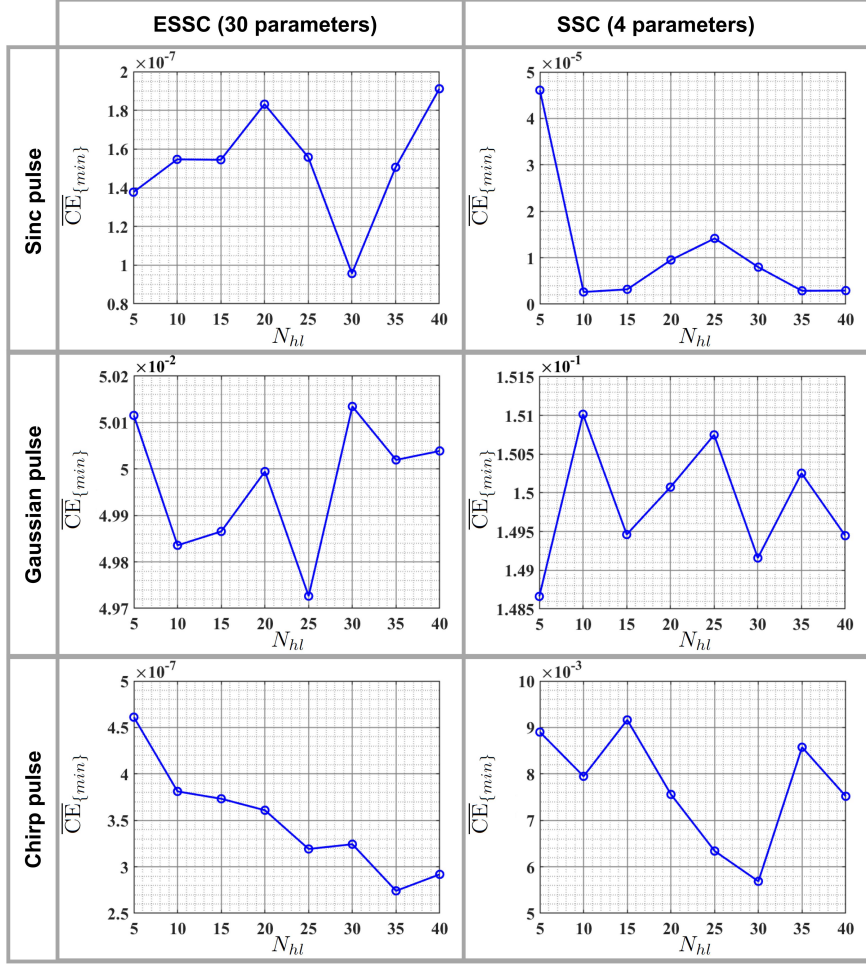


Figure 6: Minimum average cross-entropy ($\overline{CE}_{\{min\}}$) vs. the number of hidden neurons (N_{hl}) for the ANN training (with 50 different training cycles for a fixed value N_{hl}). It is shown the results for the Sinc-, Gaussian-, and Chirp-pulse pattern-recognition problems using 30- and 4-parameters methods (ESSC and SSC, respectively).

SNR	ESSC (30 parameters)						SSC (4 parameters)								
25 dB	True Class	ND	1000					True Class	ND	998				2	
		F _{G1}		1000						F _{G1}		1000			
		F _{G2}			1000					F _{G2}			999		1
		F _{LP1}				1000				F _{LP1}				1000	
		F _{LP2}					1000			F _{LP2}					1000
			ND	F _{G1}	F _{G2}	F _{LP1}	F _{LP2}			ND	F _{G1}	F _{G2}	F _{LP1}	F _{LP2}	
Predicted Class						Predicted Class									
20 dB	True Class	ND	909	2	11		78	True Class	ND	885	39	38		38	
		F _{G1}	1	999						F _{G1}	1	999			
		F _{G2}	1		994		5			F _{G2}		13	979		8
		F _{LP1}				1000				F _{LP1}				1000	
		F _{LP2}	10		176		814			F _{LP2}	70	331	255		344
			ND	F _{G1}	F _{G2}	F _{LP1}	F _{LP2}			ND	F _{G1}	F _{G2}	F _{LP1}	F _{LP2}	
Predicted Class						Predicted Class									
15 dB	True Class	ND	548	9	29		414	True Class	ND	540	116	289		55	
		F _{G1}	68	930	2					F _{G1}	27	966	7		
		F _{G2}	63		806		131			F _{G2}	37	114	834		15
		F _{LP1}			3	986	11			F _{LP1}		19	18	963	
		F _{LP2}	90	5	510		395			F _{LP2}	102	395	335		168
			ND	F _{G1}	F _{G2}	F _{LP1}	F _{LP2}			ND	F _{G1}	F _{G2}	F _{LP1}	F _{LP2}	
Predicted Class						Predicted Class									
10 dB	True Class	ND	259	105	232		404	True Class	ND	116	350	494		40	
		F _{G1}	295	654	10		41			F _{G1}	63	734	203		
		F _{G2}	43	28	777	29	123			F _{G2}	28	548	396	12	16
		F _{LP1}			112	733	155			F _{LP1}	5	104	235	638	18
		F _{LP2}	85	36	379		500			F _{LP2}	114	340	458		88
			ND	F _{G1}	F _{G2}	F _{LP1}	F _{LP2}			ND	F _{G1}	F _{G2}	F _{LP1}	F _{LP2}	
Predicted Class						Predicted Class									

Figure 7: Confusion matrix for the pattern-recognition example with a Sinc-pulse signal. The results are shown under different SNR levels of GWN, using the ESSC and SCC pre-processing algorithm in a feed-forward back-propagation ANN. The network was trained and tested with a dataset of 5000 elements (1000 elements by each class); such elements are arrays of 30- or 4-parameters for ESSC or SSC, respectively.

Confusion matrix - Gaussian pulse

SNR	ESSC (30 parameters)						SSC (4 parameters)							
25 dB	True Class	ND	907	55	32	2	4	True Class	ND	1	1	670	205	123
		F _{G1}		968	2		30		F _{G1}		400	278	147	175
		F _{G2}			997	3			F _{G2}	1	1	778	144	76
		F _{LP1}				2	998		F _{LP1}				1	999
		F _{LP2}				1	999		F _{LP2}				1	999
			ND	F _{G1}	F _{G2}	F _{LP1}	F _{LP2}			ND	F _{G1}	F _{G2}	F _{LP1}	F _{LP2}
	Predicted Class						Predicted Class							
20 dB	True Class	ND	556	128	179	30	107	True Class	ND	1	52	738	121	88
		F _{G1}	3	857	43	14	83		F _{G1}		463	275	95	167
		F _{G2}	9	3	909	51	28		F _{G2}	1	31	830	80	58
		F _{LP1}		1		3	996		F _{LP1}		1		2	997
		F _{LP2}		1		2	997		F _{LP2}		1		1	998
			ND	F _{G1}	F _{G2}	F _{LP1}	F _{LP2}			ND	F _{G1}	F _{G2}	F _{LP1}	F _{LP2}
	Predicted Class						Predicted Class							
15 dB	True Class	ND		1	1	203	795	True Class	ND		4		17	979
		F _{G1}		69		5	926		F _{G1}		69		15	916
		F _{G2}	24	42	658	194	82		F _{G2}	6	428	517	10	39
		F _{LP1}		1		97	902		F _{LP1}		1		16	983
		F _{LP2}	20	82	14	74	810		F _{LP2}		112	28	39	821
			ND	F _{G1}	F _{G2}	F _{LP1}	F _{LP2}			ND	F _{G1}	F _{G2}	F _{LP1}	F _{LP2}
	Predicted Class						Predicted Class							
10 dB	True Class	ND		117	31	79	773	True Class	ND		178	10	9	803
		F _{G1}		337	44	36	583		F _{G1}		320	25	13	642
		F _{G2}		40	57	213	690		F _{G2}		142	6	15	837
		F _{LP1}		65	6	42	887		F _{LP1}		103	10	6	881
		F _{LP2}		10	1	30	959		F _{LP2}		13	1	1	985
			ND	F _{G1}	F _{G2}	F _{LP1}	F _{LP2}			ND	F _{G1}	F _{G2}	F _{LP1}	F _{LP2}
	Predicted Class						Predicted Class							

Figure 8: Confusion matrix for the pattern-recognition example with a Gaussian-pulse signal. The results are shown under different SNR levels of GWN, using the ESSC and SSC pre-processing algorithm in a feed-forward back-propagation ANN. The network was trained and tested with a dataset of 5000 elements (1000 elements by each class); such elements are arrays of 30- or 4-parameters for ESSC or SSC, respectively.

Confusion matrix - Chirp pulse

SNR	ESSC (30 parameters)						SSC (4 parameters)							
25 dB	True Class	ND	999		1			True Class	ND	274	713	8	5	
		F _{G1}		999	1				F _{G1}	2	984	14		
		F _{G2}			1000				F _{G2}			1000		
		F _{LP1}				1000			F _{LP1}				976	24
		F _{LP2}					1000		F _{LP2}					1000
			ND	F _{G1}	F _{G2}	F _{LP1}	F _{LP2}			ND	F _{G1}	F _{G2}	F _{LP1}	F _{LP2}
	Predicted Class						Predicted Class							
20 dB	True Class	ND	937	34	26	3		True Class	ND	124	809	18	49	
		F _{G1}		994	5	1			F _{G1}	9	910	65	11	5
		F _{G2}			996		4		F _{G2}	2		993	3	2
		F _{LP1}				991	9		F _{LP1}			2	951	47
		F _{LP2}					1000		F _{LP2}					1000
			ND	F _{G1}	F _{G2}	F _{LP1}	F _{LP2}			ND	F _{G1}	F _{G2}	F _{LP1}	F _{LP2}
	Predicted Class						Predicted Class							
15 dB	True Class	ND	815	101	76	8		True Class	ND	213	753	5	29	
		F _{G1}	5	916	53	26			F _{G1}	199	726	47	25	3
		F _{G2}	5	40	930	10	15		F _{G2}	55	102	835	8	
		F _{LP1}				987	13		F _{LP1}			1	955	44
		F _{LP2}				4	996		F _{LP2}	8		29	9	954
			ND	F _{G1}	F _{G2}	F _{LP1}	F _{LP2}			ND	F _{G1}	F _{G2}	F _{LP1}	F _{LP2}
	Predicted Class						Predicted Class							
10 dB	True Class	ND	230	10	139	609	12	True Class	ND	47	448	4	494	7
		F _{G1}	5	562	159	245	29		F _{G1}	263	476	93	128	40
		F _{G2}	4	85	563	124	224		F _{G2}	125	172	565	108	30
		F _{LP1}				730	270		F _{LP1}			77	763	160
		F _{LP2}				15	985		F _{LP2}	1		236	43	720
			ND	F _{G1}	F _{G2}	F _{LP1}	F _{LP2}			ND	F _{G1}	F _{G2}	F _{LP1}	F _{LP2}
	Predicted Class						Predicted Class							

Figure 9: Confusion matrix for the pattern-recognition example with a Chirp-pulse signal. The results are shown under different SNR levels of GWN, using the ESSC and SSC pre-processing algorithm in a feed-forward back-propagation ANN. The network was trained and tested with a dataset of 5000 elements (1000 elements by each class); such elements are arrays of 30- or 4-parameters for ESSC or SSC, respectively.

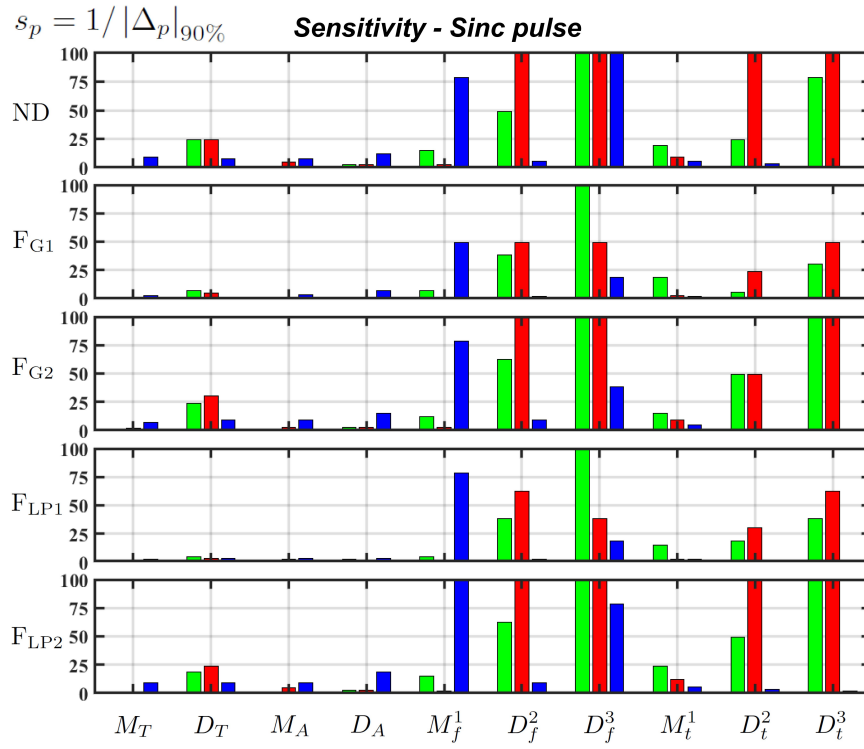


Figure 10: Sensitivity ($s_p = 1/|\Delta_p|_{90\%}$) of each ESSC parameter for the Sinc pattern recognition example. Middle red bar: signal, left green bar: derivative, right blue bar: integral.

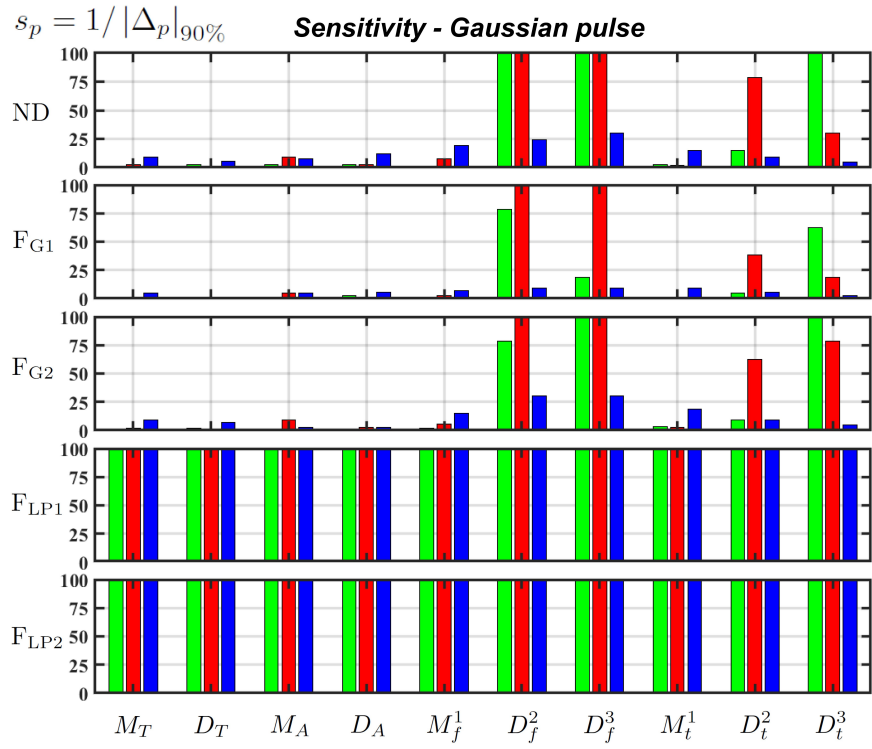


Figure 11: Sensitivity ($s_p = 1/|\Delta_p|_{90\%}$) of each ESSC parameter for the Gaussian pattern recognition example. Middle red bar: signal, left green bar: derivative, right blue bar: integral.

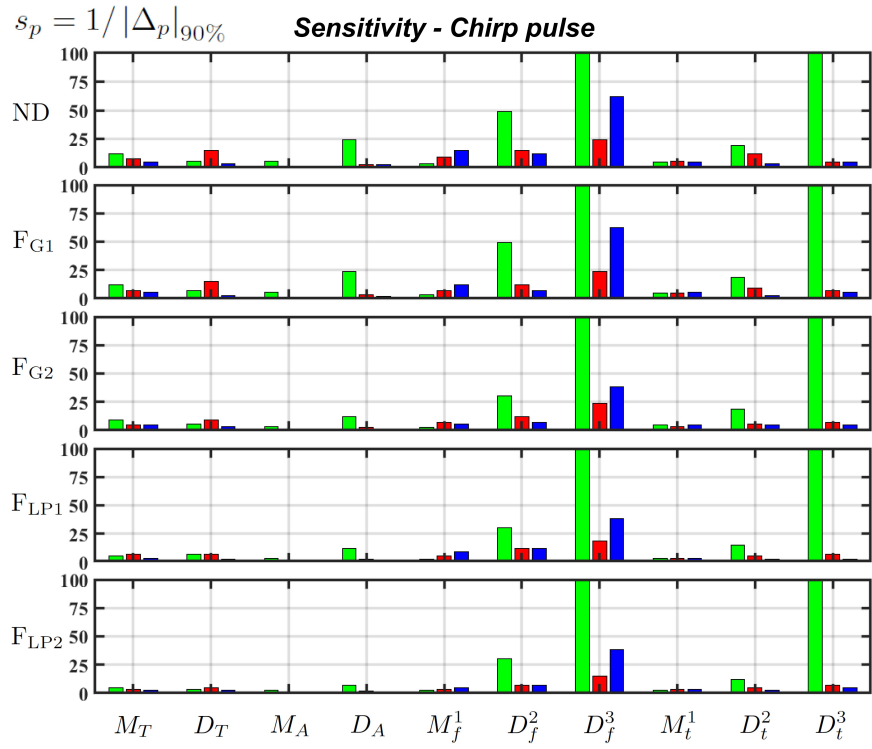


Figure 12: Sensitivity ($s_p = 1/|\Delta_p|_{90\%}$) of each ESSC parameter for the Chirp pattern recognition example. Middle red bar: signal, left green bar: derivative, right blue bar: integral.

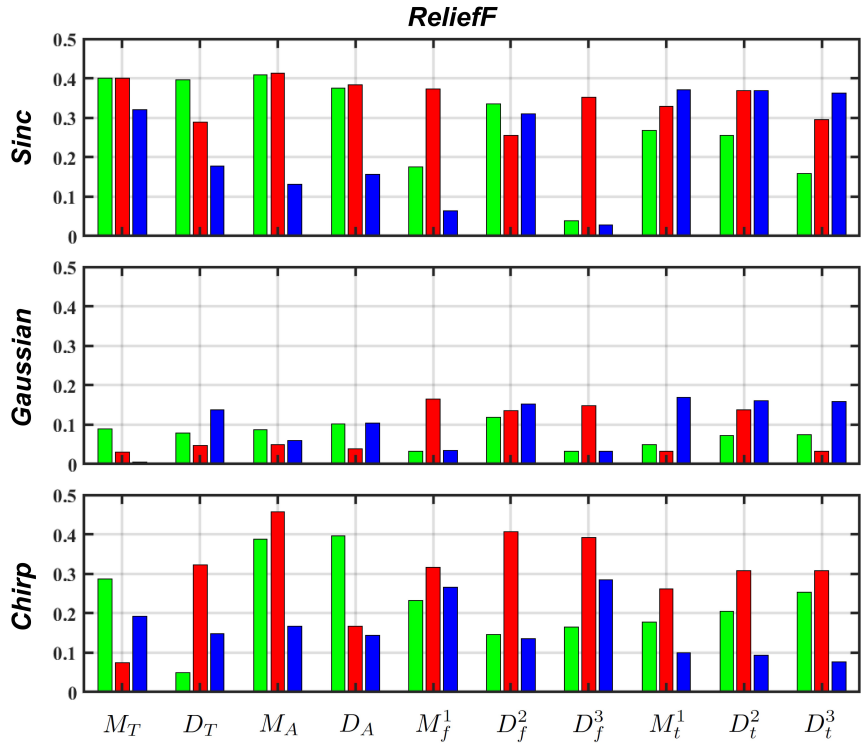


Figure 13: MATLAB® ReliefF function values of each ESSC parameter for the Sinc, Gaussian, and Chirp pattern recognition example, for classification with the parameter $K = 10$. Middle red bar: signal, left green bar: derivative, right blue bar: integral.